Imaging activated T cells predicts response to cancer vaccines

Israt S. Alam[1,2*], Aaron T. Mayer[1,2,3*], Idit Sagiv-Barfi[4], Kezheng Wang[1,5], Ophir Vermesh[1,2], Debra K. Czerwinski[4], Emily M. Johnson[1,2,6], Michelle L. James[1,2,6], Ronald Levy[4] and Sanjiv S. Gambhir[1,2]

[1]Department of Radiology, Stanford University, Stanford, CA, 94305, USA
[2]Molecular Imaging Program at Stanford, Stanford University, Stanford, CA, 94305, USA
[3]Department of Bioengineering, Stanford University, Stanford, CA, 94305, USA
[4]Division of Oncology, Department of Medicine, Stanford University, Stanford, CA, 94305, USA
[5]Department of Radiology, the Fourth Hospital of Harbin Medical University and Molecular Imaging Center of Harbin Medical University, Harbin, China
[6]Department of Neurology and Neurological Sciences, Stanford University, Stanford, CA, 94305, USA

** Authors contributed equally.*

SUPPLEMENTARY METHODS

Cell culture

All cell culture media, fetal bovine serum (FBS), penicillin/streptomycin and antibiotic/ antimycotic were obtained from Invitrogen Life Technologies. The A20 cell line, a BALB/c B cell lymphoma, CT26, a C57BL/6 murine colorectal carcinoma and 4T1, a murine mammary carcinoma were obtained from the ATCC (Manassas, VA). GL26 a murine glioma line was a kind gift from Dr. Gerald Grant (Stanford University, Stanford, CA). NDL, a murine mammary cell line were a kind gift from Katherine Ferrara (University of California Davis, Davis, CA). A20 cells were cultured as described previously (1) in RPMI 1640 medium supplemented with 10% heat-inactivated FCS (HyClone Laboratories, Logan, UT), 100 U/mL penicillin, 100µg/mL streptomycin, and 50 µM 2-ME (Sigma-Aldrich, St Louis, MO). Cells were grown in suspension and maintained at 37°C in 5% CO_2. 4T1 and CT26 cells were both cultured in RPMI 1640 medium supplemented with 10% heat-inactivated FBS and 100 U/mL penicillin, 100µg/mL streptomycin. NDL cells were cultured in complete Dulbeccos Modified Eagle Media (DMEM), supplemented with 10% heat-inactivated FBS and 100 U/mL penicillin, 100µg/mL streptomycin. Gl26 cells were also cultured in DMEM media supplemented with 10% FBS, 2mM sodium pyruvate (Invitrogen Life Technologies) and antibiotic/antimycotic.

Primary T cell isolation and activation

Murine primary T cells were isolated from the spleens of female Balb/c mice (Charles River) using a negative selection EasySep Mouse T Cell Isolation Kit (Stemcell Technologies). Purified T cells were maintained for 2 days in RPMI-1640 supplemented with 10% FBS and 1% penicillin/streptomycin at a seeding density of $4x10^6$ cells/ml. For activation, the isolated murine T cells were incubated with mouse T-Activator (CD3/CD28 specific antibody coated) Dynabeads® as per the manufacturer's instructions (a bead: cell ratio of 1:1 was used; Life Technologies, Grand Island, NY). In addition, a non-specific activation stimuli was also used and Phorbol 12-myristate 13-acetate (PMA,) (Abcam) and Ionomycin (Abcam) were added to cells at a concentration of 10 ng/ml and 100ng/ml respectively. Tracer uptake experiments or FACS analysis were performed 48 hours after activation.

Human peripheral blood mononuclear cells (PBMCs) were obtained from freshly obtained buffy coat fractions (Stanford Blood Center) using Ficoll-Paque Plus following the manufacturer's instructions (GE Healthcare). T cells were isolated (at >95% purity as determined by CD3 expression) via magnetic-activated cell sorting (MACS) using the Naïve Pan T Cell Isolation Kit per the manufacturer's instructions (Stemcell Technologies) and activated with a non-specific

activation stimuli method; Phorbol 12-myristate 13-acetate (PMA) (Abcam) and Ionomycin (Abcam) were added at a concentration of 10 ng/ml and 100ng/ml respectively. Cells were used for FACs analysis, 48 hours post initiation of activation.

Competitive binding assay

Murine T cells were isolated and activated with PMA and Ionomycin as described earlier. Activated murine T cells (1x10^6) were resuspend in FACS buffer (PBS + 2%BSA) and added to a 96 well plate. For our competitive cell binding assays, serial dilutions of OX40 mAb (clone: OX86, BioXcell), DOTA conjugated OX40 mAb, or recombinant mOX40 ligand (R&D Systems), were performed in replicate ranging in concentration from 10^{-6} M to 10^{-9} M. In addition, all wells except unstained controls were incubated with 2ul of BV421 OX40 (0.1mg/ml, clone: OX86, Biolegend) antibody for 1h at room temperature. Cells were spun down at 2000 rpm for 2 minutes and washed with FACS buffer, prior to being resuspended and analyzed for BV421 fluorescence intensity on a BD LSRII cytometer.

Radioligand cell binding assay

Murine primary T cells (activated and resting samples) were counted and prepared at a concentration of 0.5 x10^6/ml in 1 ml of pre-warmed complete media (RPMI-1640). Cells were then incubated with tracer (5 µCi) at 37°C, 5% CO_2 for 1 hour to measure uptake. For blocking studies, cells were incubated with 100 µg of anti-mouse OX40 mAb (BioXcell) for 30 minutes prior to tracer incubation. Cells were then centrifuged at 300g for 5 minutes, placed on ice and the supernatant discarded. Cells were washed twice with 1 ml ice-cold PBS, centrifuged after each wash as above and the supernatant discarded. Finally, cells were resuspended in 500µl cold PBS. 300µL was transferred to gamma counting tubes and counted on an automated gamma counter (Cobra II; Packard) to measure cell associated radioactivity. The remaining cells were used to obtain a cell count using an automated cell counter (Nexcelom Bioscience, Lawrence, MA). Data was expressed as % of total tracer added/10^5 cells. The above was repeated for murine cancer cell lines.

Fluorescence-activated cell sorting (FACS) analysis of cells and tissue

FACS analysis of tissues was performed either 2 days or 9 days after the first intra-tumoral therapy administration. Mice were anesthetized with 2.5% isoflurane gas and blood was collected by terminal cardiac puncture and subsequently added to ammonium chloride lysis buffer (Thermo Fisher Scientific). This was left at room temperature for 10 minutes. Tumors, lymph nodes and spleen were obtained and dissociated gently by pushing through a 40µm strainer to achieve a single cell suspension. Both blood and dissociated tissue samples then underwent standard wash steps for flow cytometry and cells counted prior to staining.

Murine cells were first stained with a LIVE/DEAD aqua fixable cell stain (Molecular Probes L34957) used as per the manufacturer's instructions to distinguish between live and dead cells. Cells were then washed in FACS buffer (PBS and 2% BSA) and stained with the following murine antibodies; cell surface marker specific antibodies CD3-APC (hamster IgG1 k, clone:145-2C11, BD Biosciences), CD4-APC-Cy7 (rat IgG2b k, clone GK1.5:, Biolegend) and CD8-PE (rat IgG2a k, clone: 53-6.7, Biolegend), and activation marker specific antibodies; CD25-PE-Cy7 (rat IgG1 γ, clone: PC61, BD Biosciences) CD44-PerCP-Cy5.5 (rat IgG2b k, clone: 1M7, BD Biosciences) and OX40-BV421 (rat IgG1 k, clone: OX-86, Biolegend). Prior to immunostaining of *ex vivo* samples, Fc receptors were blocked to prevent nonspecific binding for 10 min with anti-CD16/32 (rat, clone: 2.4G2, BD Biosciences).

Human T cells were stained with the following human antibodies in addition to the LIVE/DEAD fixable dead cell stain; CD3-FITC (mouse IgG2 ak, BW264/56 Miltenyi Biotech), CD4-PerCP-Cy5.5 (mouse IgG1 k, clone: RPA-T4, BD Biosciences), CD8-PE-Cy7 (mouse IgG1 k, clone: RPA-T8: , BD Biosciences) and activation marker specific antibodies CD69-PE (mouse IgG1 clone: FN50, Miltenyi Biotech) and OX40-BV605 (mouse IgG 1k /Ber-ACT35, Biolegend). All cells were fixed in 2% paraformaldehyde, stored at 4°C and analyzed within a week with the appropriate compensation control beads (ThermoFisher) using the LSR II flow cytometer (BD Biosciences). Data were analyzed using FlowJo software. For viSNE plots, cells were first gated on live and singlets and then down-sampled prior to visualization with the built in tSNE module in FlowJo. Clustering parameters included CD3, CD4, CD8, CD25, CD44, PD1, and OX40. Additional settings for computation were as follows: iterations = 1000; perplexity = 20, learning rate = 200, theta = 0.5.

Luminex® analysis of cytokines in mouse plasma

Mice were anesthetized with 2.5% isoflurane gas and 400µL blood was obtained via terminal cardiac puncture and placed in EDTA coated blood collection tubes (BD Biosciences). The tube was inverted a few times and subsequently centrifuged at 400-500 rcf at room temperature for 10 minutes. Plasma was carefully removed from the tube and placed in a clean eppendorf tube and frozen and stored at -80°C until analysis.

Plasma were analyzed for cytokines by the Stanford Human Immune Monitoring Core facility with a 38-plex murine Luminex® array (eBiosciences/Affymetrix), used according to the manufacturers' instructions. Briefly, beads were added to a 96 well plate and washed in a Biotek ELx405 washer. Frozen plasma amples were defrosted, diluted (1:3) and subsequently added to the plate containing the mixed antibody-linked beads. The sample and beads were incubated together and

placed on a orbital shaker at 500-600 rpm, first at room temperature for 1 hour before an overnight incubation at 4°C also with shaking. Plates were washed the next day in a Biotek ELx405 washer and biotinylated detection antibody added for 75 minutes at room temperature with shaking. The plate was washed as above and streptavidin-PE added. After a 30 minute incubation at room temperature, a wash was performed as above and reading buffer added to the wells. Each sample was measured in duplicate. Plates were read using a Luminex 200 instrument with a lower bound of 50 beads per sample per cytokine. Custom assay Control beads by Radix Biosolutions were added to all wells.

For Luminex® cytokine expression data, samples were run in duplicate ($n \geq 4$/group) and statistical analyses were performed based on the MFI of each sample replicate normalized to the average MFI of control replicates. Heat maps were generated in R (v3.3.3) based on $\log_2$ fold change in cytokine expression of a given experimental replicate compared to control. Unsupervised hierarchical clustering was performed using Euclidian distance and Ward's linkage. To identify significantly upregulated cytokines, significance analysis of microarrays (SAM) was applied with a false discovery rate of < 0.01.

To add biological context to the clusters identified by unsupervised hierarchical clustering, cytokine gene ontology analysis was performed in R (v3.3.3). Using Entrez gene IDs, the Ensembl database was queried and cytokines were annotated using the biological processes nomenclature. Over representation analysis was performed using the one-sided Fisher's exact test. Annotations for cytokines in cluster 1, 2, or 3 were compared relative to the total number of cytokines in the Luminex cytokine panel.

Classification and prediction of tumor response

We classified mice into two labeled groups with the help of unsupervised hierarchical clustering. To determine the cut point, we randomly selected a subset of mice (training cohort), and clustered their tumors based on their tumor growth over the study window. Based on this, tumors exhibiting less than 0.03 log fold change in tumor volume were considered responders, while tumors exhibiting greater tumor growth were considered non-responders. These class labels conformed with reasonable definitions for treatment response and subsequently provided the optimal classification results in this study. We next performed k-means clustering based on our imaging biomarkers for our training cohort and determined that the mean %ID/g tracer uptake in the tumor, tumor draining lymph node, and tumor draining lymph node normalized to tumor volume, provided the best delineation of tumors as responders or non-responders. We fixed the centroids of these clusters and then tested the performance of our simple classifier on an independent test cohort, as well as all cohorts included in our study. Assignments to response

groups were made based on Euclidian distance from the cluster centroid. All analyses were performed in R (v3.3.3).

Histology

Tumors were harvested and fixed in 4% PFA on the day of culling. After 16 hours later, tumor samples were transferred to 2% sucrose and stored at 4 degrees C. Prior to sectioning, tumors were transferred to OCT and frozen on dry ice. Sectioning and Immunofluorescent staining were performed independently by HistoTec Laboratory Inc. (Hayward, California). Samples were stained for DAPI, CD3 and OX40, excluding negative, single stain, primary, and secondary only controls.

In situ vaccine in OX40 knock out mouse model

An OX40 knockout (KO) model was employed to demonstrate the specificity of the radioligand *in vivo*. Six to eight-week-old female B6.129S4-Tnfrsf4tm1Nik/J (also known as OX40 KO) mice were purchased from JAX Laboratories. B16-F10 tumor cells (0.05×10^6) were injected subcutaneously at sites on both right and left shoulder of the mice. B16-F10 bearing tumors underwent the same treatment as in the A20 tumor model (50μg CpG in 50 μL PBS) in the tumor on the left shoulder. Mice in the control group received a 50 μL injection of PBS into the left shoulder tumor. Mice were then used for PET imaging.

SUPPLEMENTARY REFERENCES

1. Houot R & Levy R (2009) T-cell modulation combined with intratumoral CpG cures lymphoma in a mouse model without the need for chemotherapy. *Blood* 113(15):3546-3552.

SUPPLEMENTARY FIGURE LEGENDS

Supplementary Figure 1. ***Tracer synthesis and quality control schematic. A)*** Synthesis schema ***B)*** Conjugation results with representative mass spectrometry histograms. ***C)*** Competitive binding assay between the OX40 antibody and DOTA conjugated mAb or endogenous OX40 ligand (OX40L) using activated murine T cells ***D)*** Gel of unconjugated stock antibody showing bands corresponding to 150kDa and 50kDa (lane 1), antibody sample post DOTA conjugation (lane 2) and HPLC peak product (lane 3) ***E)*** Radio-HPLC ***F)*** Final tracer synthesis results.

Supplementary Figure 2. ***Study design.*** Timeline and schedule for therapy, blood draws, imaging and biopsies (d=day).

Supplementary Figure 3. ***FACS gating and supporting data. A)*** FACS plot representation of the gating strategy employed throughout this study. ***B)*** Mean frequency of OX40+ CD3 T cells in tumor and tumor draining lymph node (TDLN). One-way ANOVA with Bonferroni post-test. ***, $p < 0.001$; **, $p < 0.01$; *, $p < 0.05$. Representative FACS plots from Tumor and TDLN of CPG and Vehicle (Veh) cohorts respectively. Values on plots represent % of CD3 T cells. ***C)*** Freq of CD4 and CD8 T cells in CpG vs Vehicle tumor, tumor draining lymph node and spleen at the early day 2 timepoint. ***D)*** Frequency of CD4 and CD8 T cells in CpG normalized to vehicle at early and late time points.

Supplementary Figure 4. ***Phenotypic characterization of OX40 cells. A)*** ViSNE graphs displaying biomarkers and clustering in tumor and TDLN. OX40 restricted to CD4 cluster. ***B)*** FACS plots of OX40+ or OX40- CD4+ T cells in the tumor and tumor draining lymph node (TDLN). ***C)*** CD4+ T cell phenotype in CPG treated Tumors. ***D)*** Effector (FoxP3-) vs. regulatory (FoxP3+) OX40+ CD4 T cell percentages in CPG vs Vehicle cohorts.

Supplementary Figure 5. ***Blood cytokine signature. A)*** Heat map of log2 fold change cytokine expression in vehicle and CPG mice normalized to control. Unsupervised hierarchical clustering performed on heat map rows (cytokines). Column naming key: (2/9) day of analysis; (C/V) CpG or Veh; (A/B/C) sample identifier; (1/2) sample replicate. Three primary clusters labelled as 1, 2 & 3. ***B-C)*** Tabular results of top upregulated hits from significance analysis of microarrays for day 2 and day 9 respectively. ***D-E)*** Unsupervised hierarchical clustering phylograms of CpG and Vehicle samples based on cytokine signatures from day 2 and day 9 respectively.

Supplementary Figure 6. ***Cytokine ontology*****.** ***A)*** Number of unique Entrez gene ID biological processes annotations for the three primary cytokine clusters identified by unsupervised hierarchical clustering. ***B)*** Top over representation analysis hits and respective p-values for biological processes associated with cytokine cluster 1. ***C)*** Top over representation analysis hits and respective p-values for biological processes associated with cytokine cluster 2.

Supplementary Figure 7. ***ImmunoPET imaging supporting data.*** Annotated PET/CT images from CPG, CPG + blocking and vehicle cohorts. Left: Coronal cross-sections. Right: Axial cross-sections. C.LN = cervical lymph node; A.LN = axillary lymph node; LT = left tumor; RT = right tumor; B.LN = brachial lymph node; Sp = spleen; K = kidney; B = bladder; I.LN = inguinal lymph node; P.LN = popliteal lymph node.

Supplementary Figure 8. ***Histology of CpG and vehicle treated tumors A)***. Two representative day 2 histology sections stained for DAPI (purple) and CD3 (red) from CpG and vehicle cohorts. White scale bar represents 1mm. ***B)*** Histology sections from CpG and Vehicle cohorts with OX40 (green) staining, 20x magnification of selected regions. ***C)*** CpG and vehicle histology sections at 40x magnification showing DAPI, OX40 and CD3 staining.

Supplementary Figure 9. ***Supporting ImmunoPET Quantification and Imaging Controls A)*** Unsupervised hierarchical clustering of CpG vs Vehicle mice based on imaging biomarkers. Parameters for each cluster are listed in figure. ***B)*** Early (day 2) post therapy ^{64}Cu-DOTA-AbOX40 uptake profile [%ID/g ROI; no PVC] in CpG (n=7) vs Vehicle (Veh, n=7) vs intratumoral blocking (I.T. block, n=4) and naïve (n=3) cohorts at 24 hours post tracer injection [100 µCi]. UT: untreated tumor; TT: treated tumor; Sp: spleen; Ax: axillary lymph node; Pop: popliteal lymph node; Ing: inguinal lymph node; Mus: muscle; Br: brain ***C)*** ^{64}Cu-DOTA-AbOX40 ROI vs BIOD uptake [%ID/g] in tumor, tumor draining lymph node, spleen and muscle. Black dashed line: y=x; Shaded gray zone: 95% CI ***D)*** Fold change in treated tumor uptake [%ID/g, BIOD] between CpG and control groups [Vehicle, Intravenous (i.v.) blocking, & Intravenous isotype]. ***E)*** Fold change in treated vs untreated tumor uptake [%ID/g] BioD in CpG treated wt mice and CpG treated OX40 k/o mice. All values represent mean +/- SEM unless specified. Two-way ANOVA with Bonferroni post-test for multiple comparisons; else student's t-test ****, $p < 0.0001$; ***, $p < 0.001$; **, $p < 0.01$; *, $p < 0.05$, ns = not significant.

Supplementary movie 1. CPG mouse imaged with OX40 ImmunoPET (day 2 post therapy, 24h post tracer injection)

Supplementary movie 2. Vehicle mouse imaged with OX40 ImmunoPET (day 2 post therapy, 24h post tracer injection)***.***

SUPPLEMENTARY FIGURES

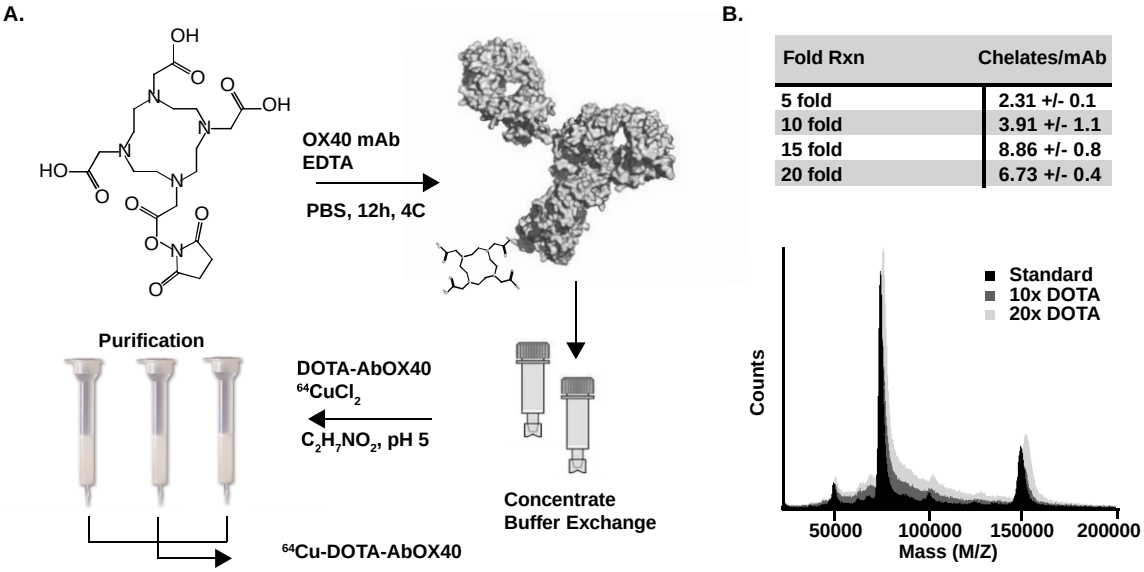

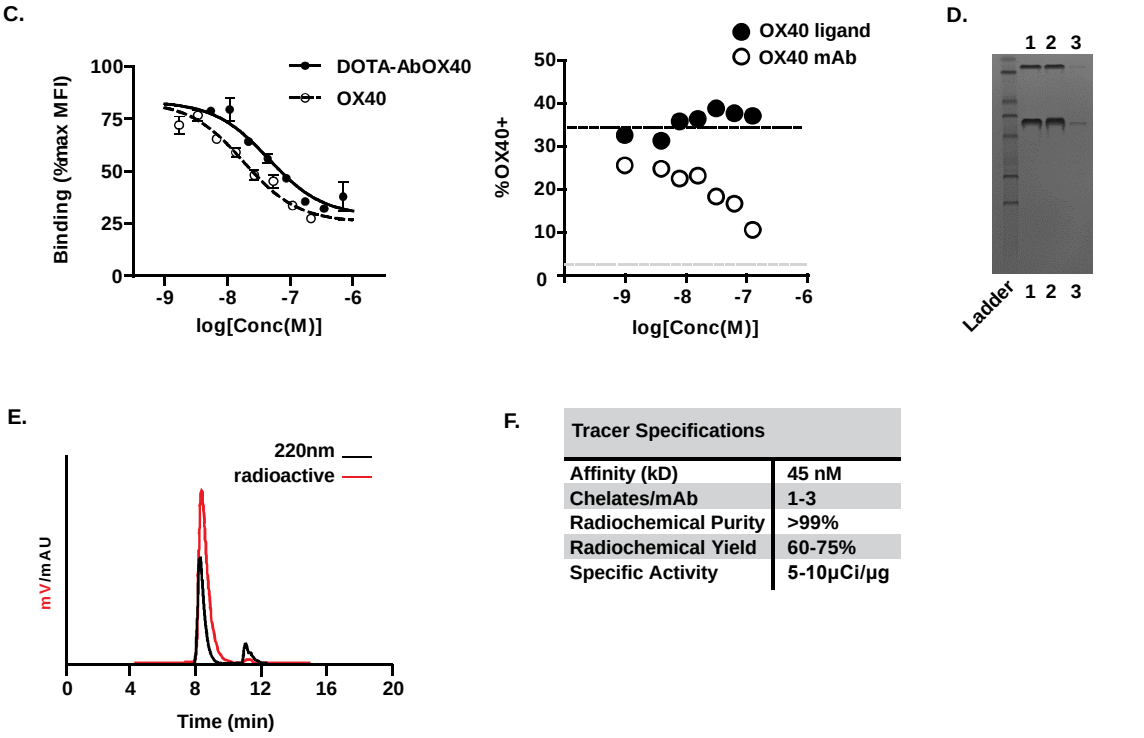

F.

Tracer Specifications	
Affinity (kD)	45 nM
Chelates/mAb	1-3
Radiochemical Purity	>99%
Radiochemical Yield	60-75%
Specific Activity	5-10μCi/μg

Supplementary Figure 1. ***Tracer synthesis and quality control schematic.***

A. Study Design

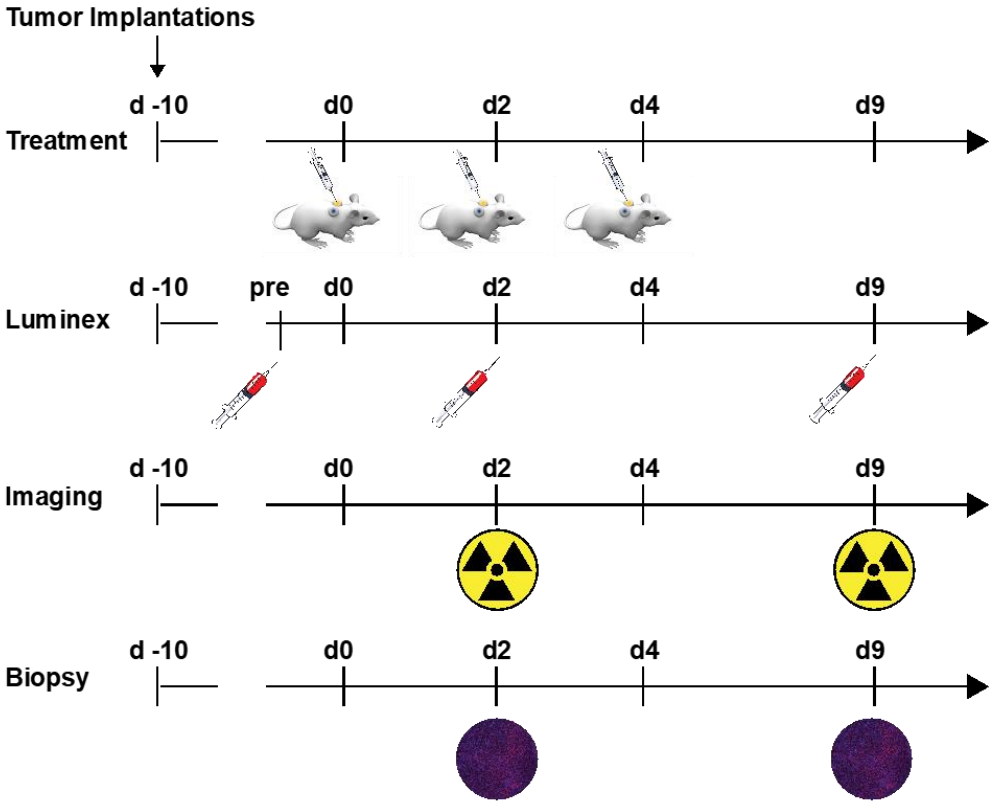

Supplementary Figure 2. ***Study design.***

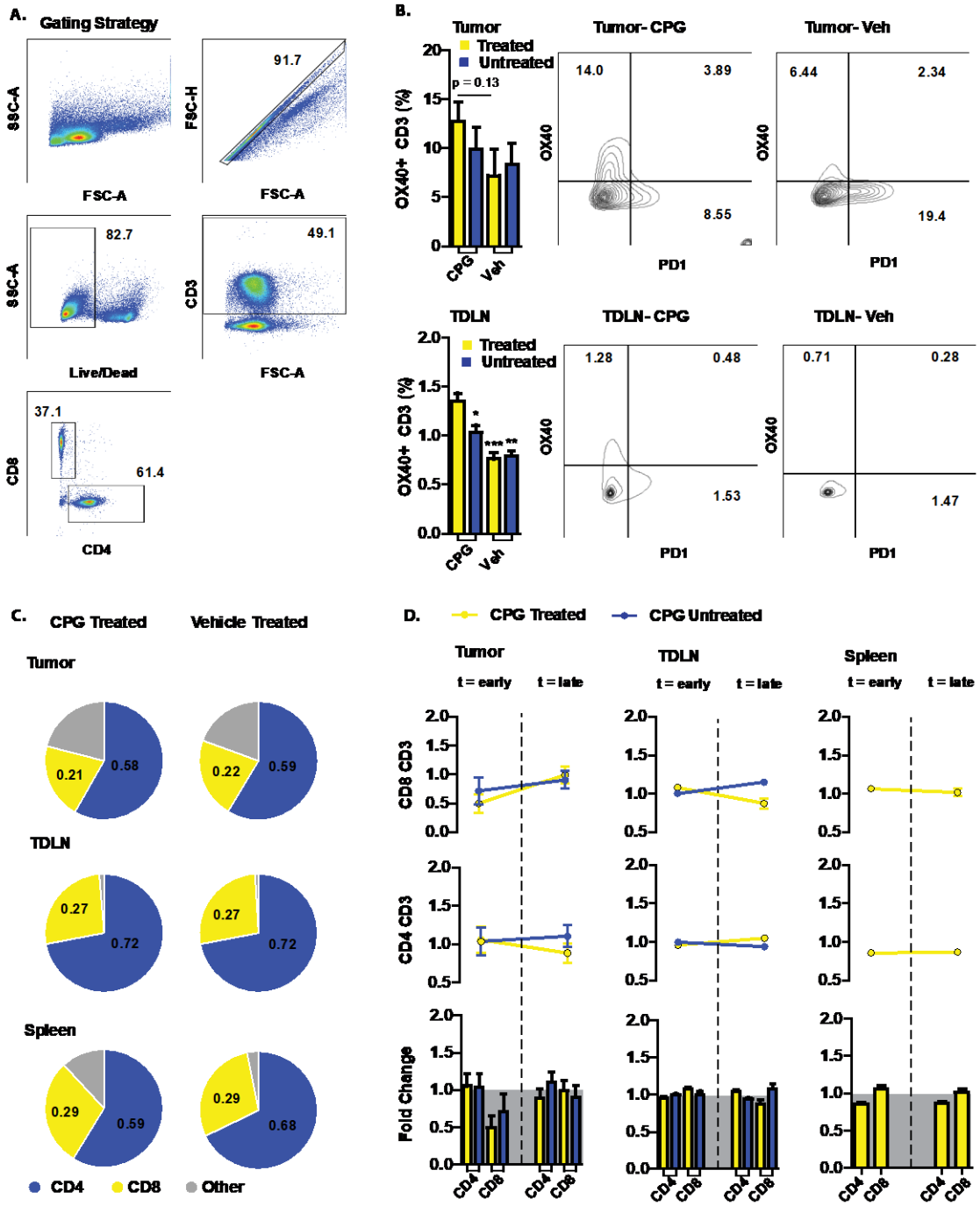

Supplementary Figure 3. ***FACS gating and supporting data.***

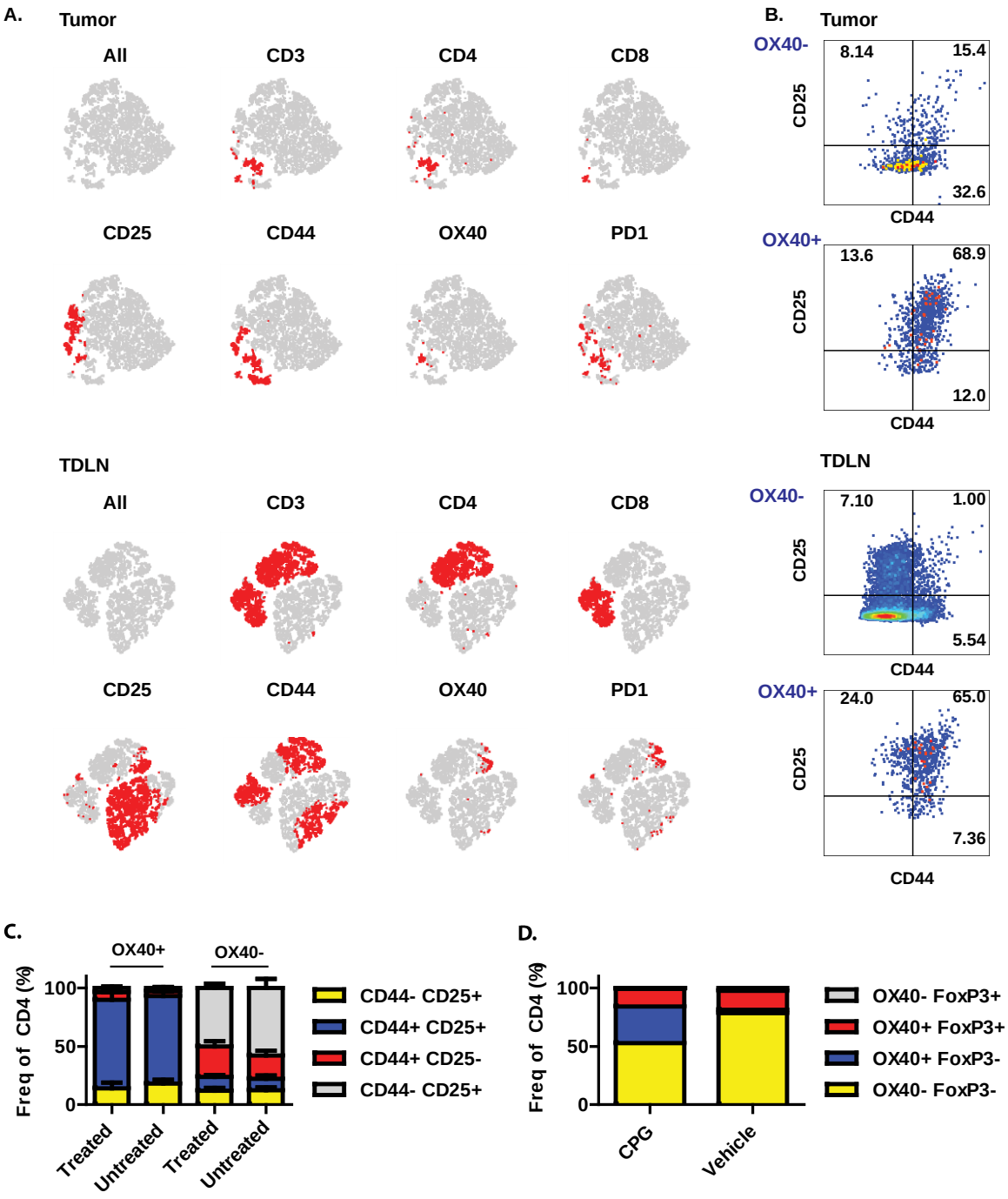

Supplementary Figure 4. ***Phenotypic characterization of OX40 cells.***

A.

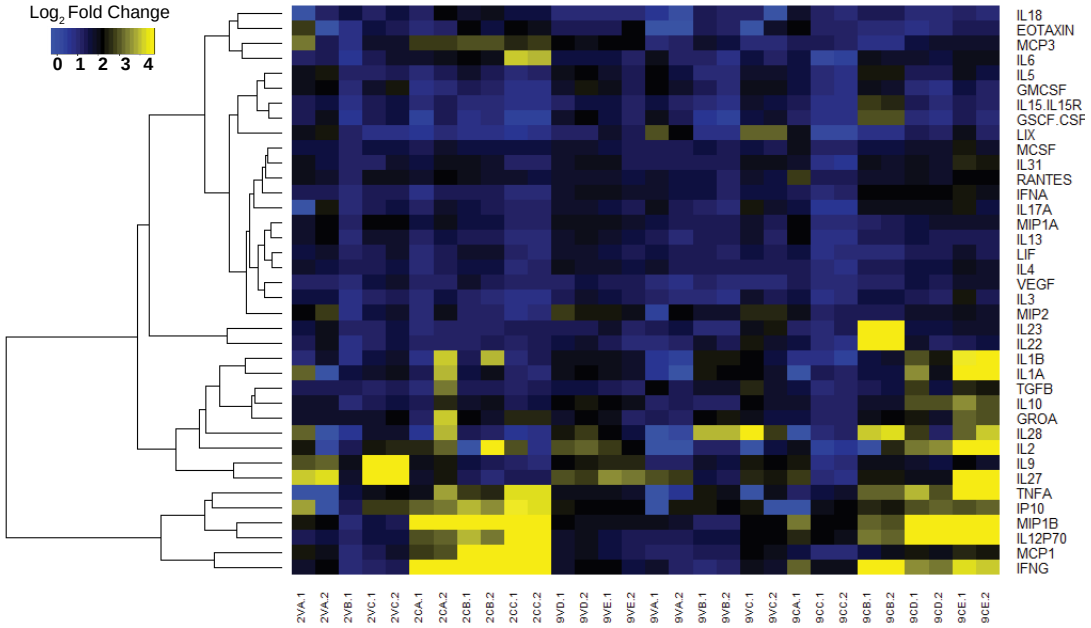

B. Day 2

ID	Score(d)	Numerator (r)	Denominator(s+s0)	Fold Change	q-value(%)
IFNG	4.439	4.783	1.077	27.534	0.000
MIP1B	4.439	3.251	0.732	9.518	0.000
IL12P70	3.259	2.263	0.694	4.800	0.000
MCP1	2.323	3.497	1.505	11.287	0.000
TNFA	2.188	1.572	0.719	2.973	0.000
IP10	1.895	1.374	0.725	2.591	0.000
IL6	1.676	1.655	0.988	3.150	0.000
MCP3	1.391	1.198	0.861	2.294	0.000
IL2	1.385	1.193	0.862	2.286	0.000
GROA	1.351	0.737	0.545	1.666	0.000
IL1B	1.162	1.092	0.940	2.132	0.000
IL18	1.085	0.794	0.732	1.734	0.000
IL10	0.682	0.394	0.577	1.314	29.934
TGFB	0.626	0.415	0.663	1.333	29.934
EOTAXIN	0.585	0.427	0.729	1.344	29.934
MCSF	0.536	0.207	0.387	1.155	29.934
RANTES	0.392	0.225	0.576	1.169	49.415
IL31	0.364	0.196	0.539	1.146	49.415
IL17A	0.246	0.117	0.474	1.084	53.759

C. Day 9

ID	Score(d)	Numerator (r)	Denominator(s+s0)	Fold Change	q-value(%)
IFNG	1.619	1.764	1.090	3.396	0.000
MIP1B	1.606	1.119	0.697	2.172	0.000
IL18	1.480	1.114	0.753	2.165	0.000
IL12P70	1.428	0.924	0.647	1.897	0.000
TNFA	0.920	1.258	1.367	2.391	50.526
IL23	0.730	1.730	2.370	3.317	104.025
RANTES	0.541	0.355	0.656	1.279	104.025
VEGF	0.515	0.233	0.452	1.175	104.025
IL22	0.506	0.731	1.445	1.660	104.025
EOTAXIN	0.477	0.329	0.691	1.256	104.025
GSCF.CSF3	0.367	0.422	1.150	1.340	104.025
IL3	0.327	0.217	0.664	1.163	104.025
IP10	0.324	0.239	0.737	1.180	104.025
IL2	0.238	0.211	0.885	1.157	104.025
IL15.IL15R	0.235	0.222	0.945	1.166	104.025
MCSF	0.216	0.108	0.501	1.078	104.025
IL10	0.163	0.106	0.648	1.076	104.025
IL1A	0.109	0.134	1.231	1.097	112.281

D. Day 2

E. Day 9

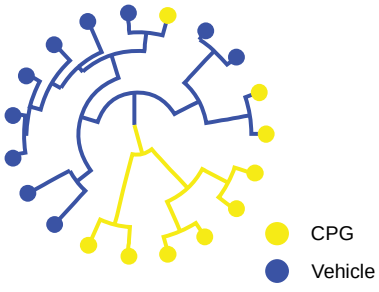

Supplementary Figure 5. ***Blood cytokine signature.***

A.

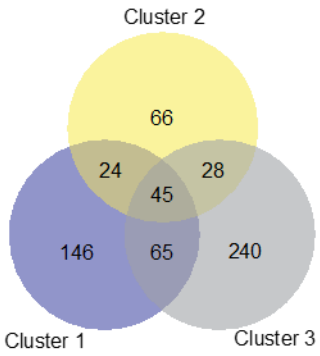

B. Cluster 1

GO: Biological Process	p-value
cell chemotaxis	0.093906
cellular response to drug	0.050134
cellular response to lipopolysaccharide	0.003472
chemokine-mediated signaling pathway	0.102337
chemotaxis	0.102337
defense response to bacterium	0.093906
extrinsic apoptotic signaling pathway	0.017825
G-protein coupled receptor signaling pathway	0.102337
humoral immune response	0.050134
negative regulation of gene expression	0.050134
negative regulation of growth of symbiont in host	0.050134
negative regulation of myoblast differentiation	0.050134
negative regulation of transcription from RNA polymerase II promoter	0.017825
negative regulation of transcription, DNA-templated	0.050134
neutrophil chemotaxis	0.102337
positive regulation of apoptotic process	0.050134
positive regulation of calcidiol 1-monooxygenase activity	0.050134
positive regulation of cell adhesion	0.006361
positive regulation of chemokine biosynthetic process	0.093906
positive regulation of membrane protein ectodomain proteolysis	0.050134
positive regulation of monocyte chemotaxis	0.050134
positive regulation of nitric oxide biosynthetic process	0.093906
positive regulation of protein complex assembly	0.017825
positive regulation of tumor necrosis factor production	0.093906
positive regulation of vitamin D biosynthetic process	0.017825
protein import into nucleus, translocation	0.017825
regulation of cell proliferation	0.093906
regulation of insulin secretion	0.093906
response to virus	0.050134

C. Cluster 2

GO: Biological Process	p-value
ectopic germ cell programmed cell death	0.037433
extrinsic apoptotic signaling pathway in absence of ligand	0.047622
fever generation	0.100602
negative regulation of cell proliferation	0.085682
negative regulation of inflammatory response	0.100602
positive regulation of angiogenesis	0.100602
positive regulation of cell division	0.037433
positive regulation of cytokine secretion	0.100602
positive regulation of interleukin-2 biosynthetic process	0.037433
positive regulation of mitotic nuclear division	0.037433
positive regulation of monocyte chemotactic protein-1 production	0.037433
positive regulation of vascular endothelial growth factor production	0.037433
response to molecule of bacterial origin	0.100602

Supplementary Figure 6. ***Cytokine ontology***

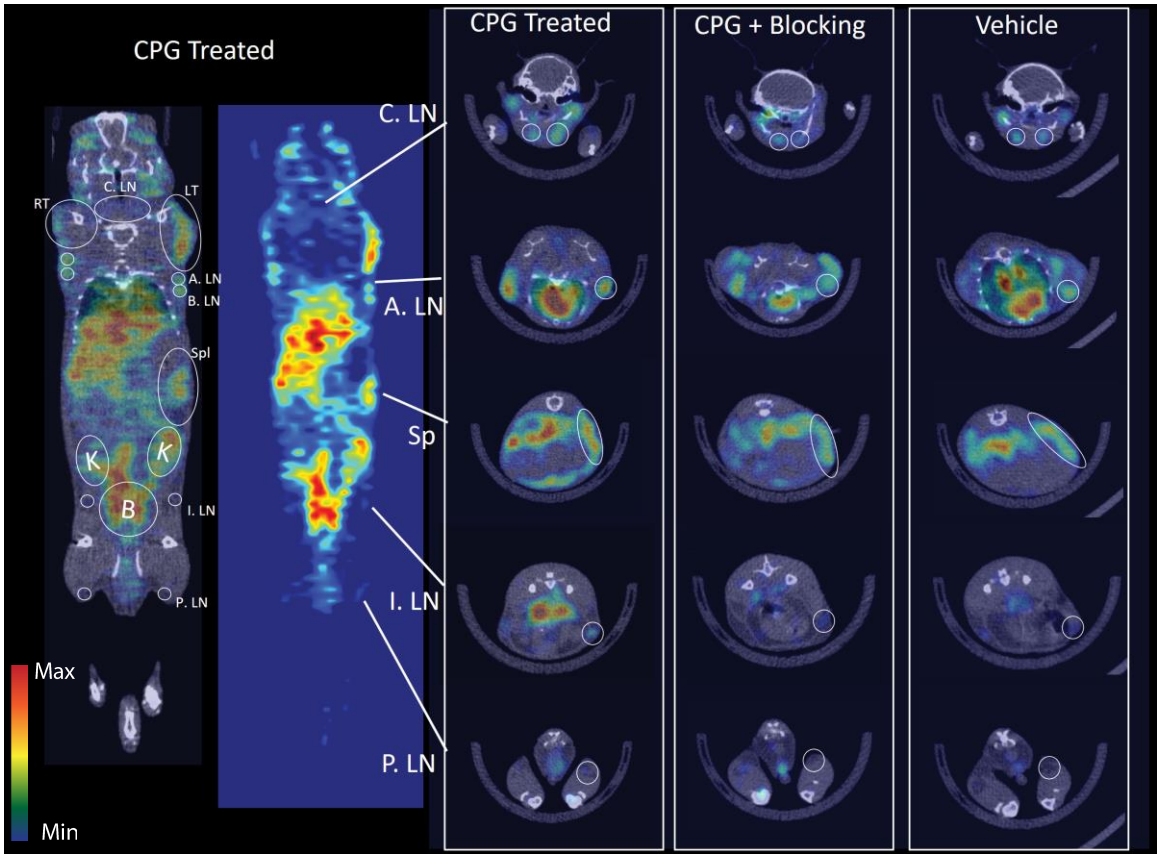

Supplementary Figure 7. ***ImmunoPET imaging supporting data.***

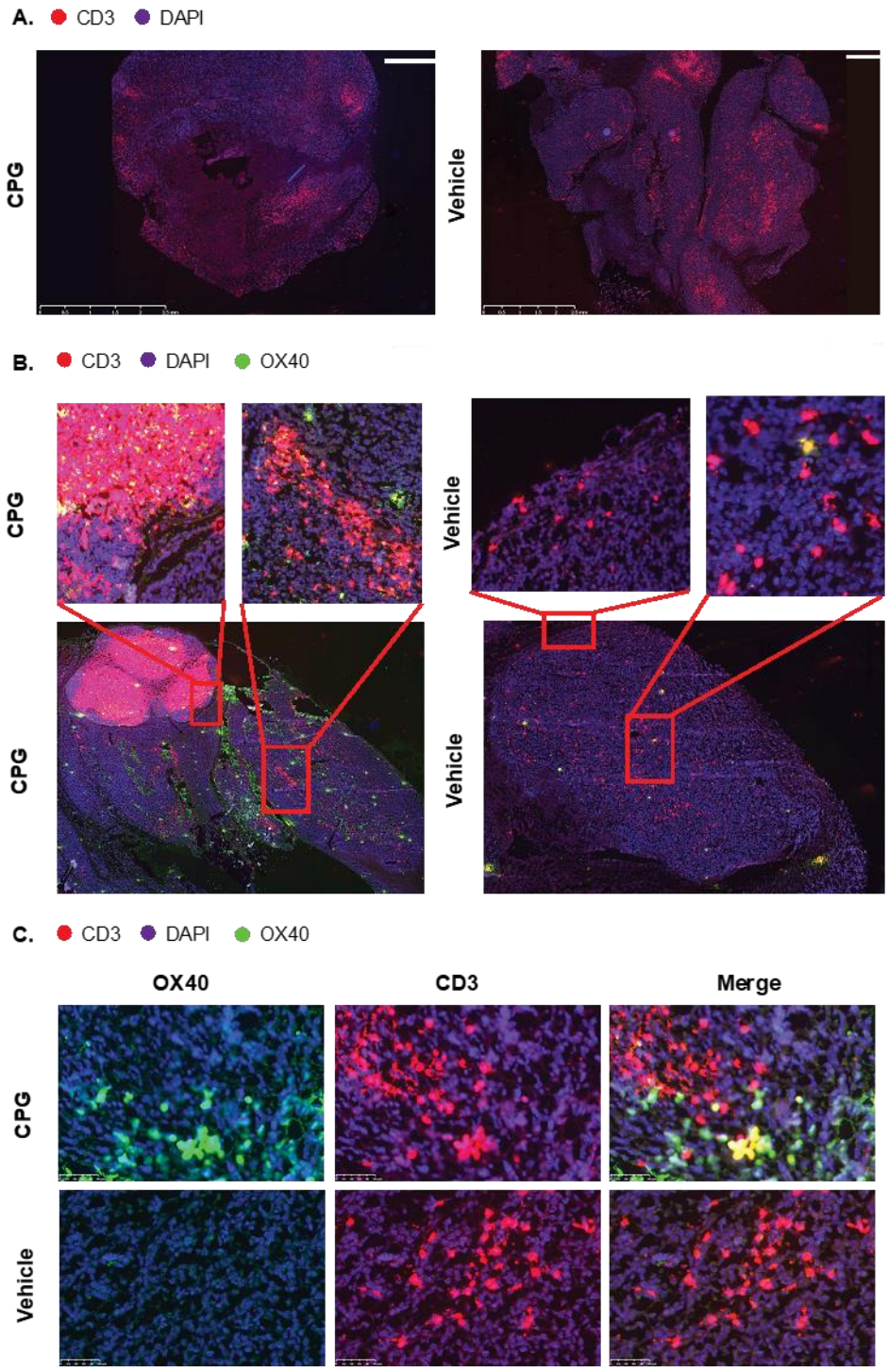

Supplementary Figure 8. ***Histology***

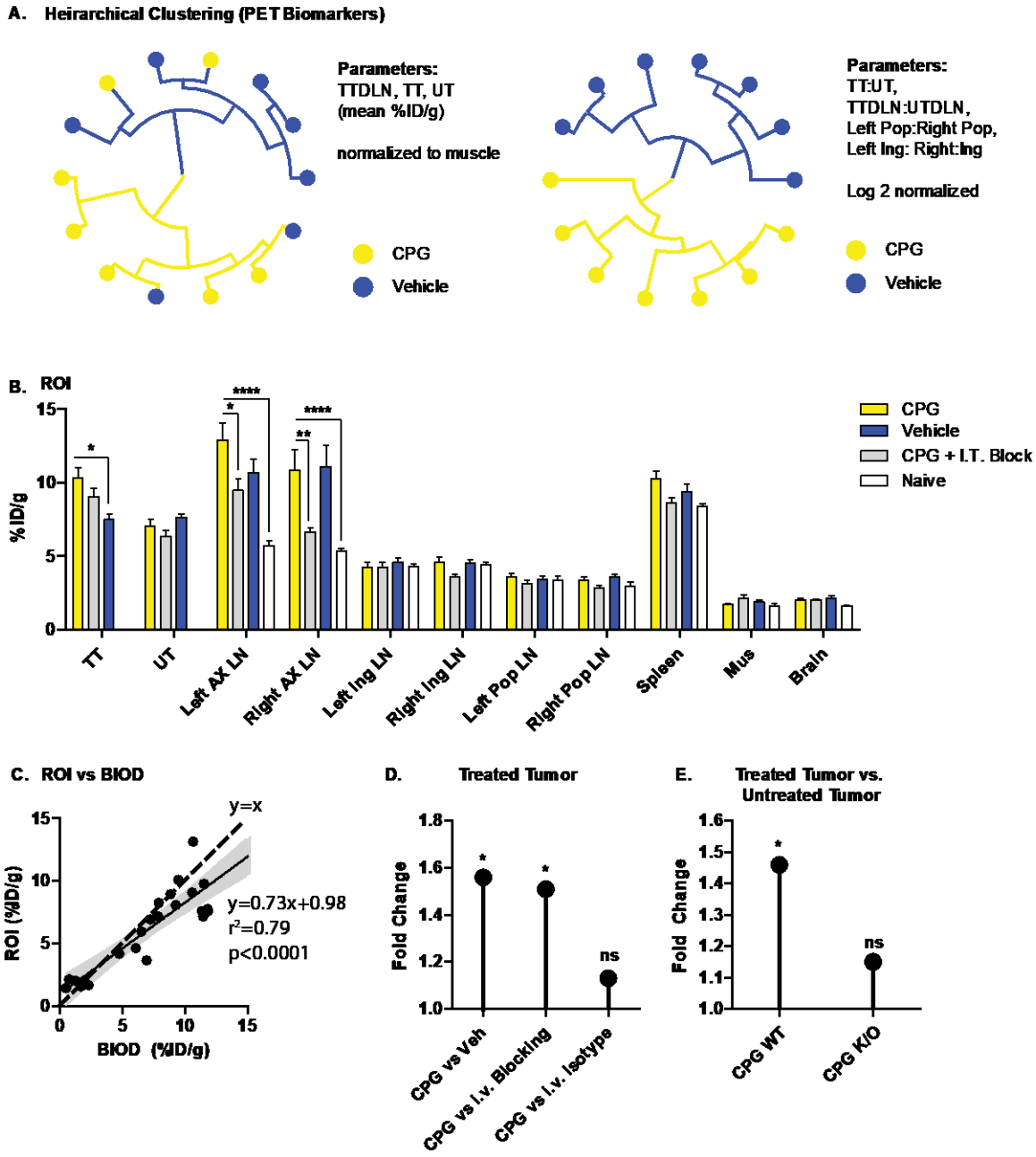

Supplementary Figure 9. ***Supporting ImmunoPET Quantification and Imaging Controls***